

Improving the Chiral Properties of Lattice Fermions

Thomas DeGrand, Anna Hasenfratz

Department of Physics, University of Colorado, Boulder, CO 80309 USA

Tamás G. Kovács

Department of Theoretical Physics, University of Pécs, H-7624 Pécs, Ifjúság útja 6, Hungary

(Dated: 6th November 2018)

The chiral properties of lattice fermions can be improved by altering either their fermion-gauge coupling or the pure gauge part of the action (or both). Using both perturbation theory and nonperturbative simulation, we compare a simple alteration of the gauge action (which encompasses the Wilson, Symanzik, Iwasaki, and DBW2 actions), and HYP-blocked links in the fermion action. Perturbative tests include calculations of the potential, flavor-changing quark scattering amplitudes, and matching factors for currents. Non-perturbative tests include the potential, measurements of flavor symmetry breaking for staggered fermions, the behavior of topological objects, and properties of overlap actions. Our results display the bad properties of these actions as well as their good ones.

I. INTRODUCTION

The chiral symmetry breaking of lattice fermions is the most serious lattice artifact we face in numerical simulations. Most dynamical simulations use staggered or Wilson-like fermions, where chiral symmetry breaking is explicit and difficult to control. In the case of staggered fermions lattice artifacts induce flavor symmetry breaking, resulting in non-Goldstone pions that can be significantly heavier than the Goldstone particle. In the case of Wilson-like fermions the effect of chiral symmetry breaking is most observable in the occurrence of exceptional configurations. Domain wall fermions, which in theory are chiral, have a residual chiral symmetry breaking due to the finiteness of the fifth lattice direction. Overlap fermions are chiral, no matter what non-chiral action they are constructed from. However, the computational requirements needed to evaluate the overlap operator can be significantly lowered if it is based on a near-chiral action.

A systematic improvement program modifies the pure gauge part of the action, the fermionic action, and the gauge connections of the fermions, to construct a chirally improved action with reduced lattice artifacts. Less ambitious programs might change only part of the action at a time, according to the improvement needs of the program.

Several possibilities have been explored to improve the chiral symmetry of fermionic actions. They are all based on the observation that most of the chiral violation come from the short scale, plaquette level vacuum fluctuations of the gauge field. One option is to smear the gauge connection of the fermions, reducing the coupling of fluctuations to the fermions. This option has been used with staggered fermions [1, 2]. The two smearing transformations that are used most extensively are the Fat7/Asqtad [3, 4, 5] and HYP smearings [6]. Both of these transformations are $O(a^2)$ perturbatively improved, though only the Asqtad smearing was designed perturbatively. The HYP smearing is optimized non-perturbatively.

The other option that has been studied lately is to modify the pure gauge action such a way that the creation of small scale vacuum fluctuations is dynamically suppressed. The Iwasaki action [7] has been used extensively by CP-PACS both in dynamical Wilson and domain wall fermion simulations [8, 9] while the DBW2 action [10, 11] was chosen by the Columbia-BNL group in their domain wall fermion simulations [12]. The Iwasaki and especially the DBW2 actions have larger perturbative lattice corrections than the Wilson plaquette action though in numerical tests that did not seem to increase the lattice artifacts.

The advantage for numerical simulations of modifying the gauge action instead of smearing the gauge connection is obvious. Almost any gauge action can be simulated faster than a complicated fermionic action, though with the recently developed partial-global stochastic Metropolis (PGSM) update even projected smeared link fermions can be

simulated effectively [2, 13, 14]. The important question is if the improvement offered by the modified gauge actions is sufficient, and even more, if, in addition to the improved chiral symmetry any unwanted lattice artifacts are introduced by these actions.

Our goal in this paper is to compare different physical properties, both perturbative and non-perturbative, of the smeared and modified gauge actions, and possibly to predict which choice is going to give the most efficient approach of the continuum limit.

In Sec. 2 we introduce the actions we study. A perturbative analysis of the properties of these actions is carried out in Sec. 3. In Sec. 4 we show simulation results for the heavy quark potential. The topological properties of these actions are discussed in Sec. 5. Flavor symmetry violations for staggered actions are shown in Sec. 6. Sec. 7 discusses some properties of overlap actions built using HYP links or in the background of gauge fields with the gauge actions we study. Our conclusions are found in Sec. 8.

II. THE ACTIONS

In the following we consider a family of actions consisting of the 1×1 plaquette and the 1×2 planar loop

$$S_g(U) = \frac{\beta}{3} [c_0 \sum_{n, \mu < \nu} W_{\mu\nu}^{1 \times 1}(n) + c_1 \sum_{n, \mu \neq \nu} W_{\mu\nu}^{1 \times 2}(n)] \quad (1)$$

with the normalization condition $c_0 + 8c_1 = 1$. The coefficient c_1 can vary, giving the different actions

$$c_1 = 0 \quad \text{Wilson} \quad (2)$$

$$-1/12 \quad \text{tree level Symanzik} \quad (3)$$

$$-0.331 \quad \text{Iwasaki} \quad (4)$$

$$-1.4088 \quad \text{DBW2.} \quad (5)$$

The tree level Symanzik action is $O(a^4)$ improved [15], while both the Iwasaki and DBW2 actions have opposite $O(a^2)$ corrections than the Wilson plaquette action. Some of the scaling properties of the Iwasaki action have been studied in [8] while the DBW2 action was investigated in [10, 12]. In our numerical simulations we use the 1-loop tadpole improved Symanzik action [16, 17]

$$S_{\text{Sym1l}}(U) = \frac{\beta_{1 \times 1}}{3} \sum_{n, \mu < \nu} W_{\mu\nu}^{1 \times 1}(n) + \frac{\beta_{1 \times 2}}{3} \sum_{n, \mu \neq \nu} W_{\mu\nu}^{1 \times 2}(n) + \frac{\beta_{pg}}{3} \sum_{n, \mu \neq \nu \neq \rho} W_{\mu\nu\rho}^{pg} \quad (6)$$

where W^{pg} is a six-link parallelogram with links running around the opposing edges of the cube. The β coefficients for S_{Sym1l} are tadpole improved according to the plaquette expectation value.

In addition to the different gauge actions we will consider two smearing transformations for the fermion-gauge field interaction. The Fat7 smearing replaces the usual one-link coupling with a linear combination of gauge loops up to length seven. It has perturbatively determined coefficients which remove the flavor changing gluons at the edges of the Brillouin zone for staggered fermions. When an additional 5-link term is added to the Fat7 smearing the resulting action is $O(a^2)$ improved in the fermion-gluon connection [3]. With tadpole boosted coefficients this leads to the Asqtad smearing transformation [5]. (One should note that the Asqtad staggered action also has a third nearest neighbor Naik term, which we do not include here.) The Asqtad smeared links are not unitary – they are simply the linear combinations of the extended gauge paths.

Our second smearing transformation is HYP smearing [6]. HYP smeared links are constructed from three levels of modified, SU(3) projected APE blocking steps in a way that makes the transformation local and smooth. While the HYP smearing is non-perturbatively optimized, its coefficients can just as well be tuned to give perturbative improvement.

III. PERTURBATIVE CONSIDERATIONS

A. Preliminaries

The gauge actions we study have propagators which obey the equation

$$\left[\frac{1}{\xi-1}\hat{k}_\mu\hat{k}_\nu + \sum_\rho(\hat{k}_\rho\delta_{\mu\nu} - \hat{k}_\mu\delta_{\rho\mu}q_{\mu\rho}\hat{k}_\rho)\right]G_{\mu\nu} = \delta_{\mu\nu} \quad (7)$$

where

$$q_{\mu\nu} = (1 - \delta_{\mu\nu})(1 - c_1(\hat{k}_\mu^2 + \hat{k}_\nu^2)) \quad (8)$$

and $\hat{k}_\mu = 2\sin(k_\mu/2)$. ξ is the gauge-fixing term: $\xi = 1$ is Feynman gauge. The Wilson gauge action propagator is

$$G_{\mu\nu} = [\delta_{\mu\nu} + (\xi - 1)\frac{\hat{k}_\mu\hat{k}_\nu}{\hat{k}^2}]\frac{1}{\hat{k}^2}. \quad (9)$$

For other actions we merely numerically invert Eq. 7 to construct the propagator.

We will be concerned only with unitary fat links, gauge connections which are themselves elements of the gauge group, even though they may be built of sums of products of the original thin links of the simulation. For smooth fields the fat links have an expansion $V_\mu(x) = 1 + iaB_\mu(x) + \dots$ and the original thin links have an expansion $U_\mu(x) = 1 + iaA_\mu(x) + \dots$. For computations of 2- and 4-quark operator renormalization/matching constants at one loop, only the linear part of the relation between fat and thin links is needed [18], and it can be parameterized as

$$B_\mu(x) = \sum_{y,\nu} h_{\mu\nu}(y)A_\nu(x+y). \quad (10)$$

Quadratic terms in (10), which would only be relevant for tadpole graphs, appear as commutators and therefore do not contribute, since tadpoles are symmetric in the two gluons. In momentum space, the convolution of Eq. (10) becomes a form factor

$$B_\mu(q) = \sum_\nu \tilde{h}_{\mu\nu}(q)A_\nu(q). \quad (11)$$

If all gluon lines start and end on fermion lines, then, effectively, the gluon propagator changes into

$$\mathcal{G}_{\mu\nu} \rightarrow \tilde{h}_{\mu\lambda}G_{\lambda\sigma}\tilde{h}_{\sigma\nu}. \quad (12)$$

Obviously, this means that in perturbation theory, as far as the fermions are concerned, fattening the links in the fermion action is equivalent to altering the gauge action.

The family of smearings including HYP links [6] and the order- a^2 improved link [3] which, when augmented by tadpole improvement, gives the ‘‘Asqtad’’ link used by the MILC collaboration [5], have

$$\tilde{h}_{\mu\nu} = \delta_{\nu,\mu}D_\mu(k) + (1 - \delta_{\nu,\mu})G_{\nu,\mu}(k). \quad (13)$$

The diagonal and off-diagonal couplings can be decomposed, respectively, as

$$D_\mu(k) = 1 - \frac{d_1}{4} \sum_{\nu \neq \mu} \hat{k}_\nu^2 + \frac{d_2}{16} \sum_{\substack{\nu < \rho \\ \nu, \rho \neq \mu}} \hat{k}_\nu^2 \hat{k}_\rho^2 - \frac{d_3}{64} \hat{k}_\nu^2 \hat{k}_\rho^2 \hat{k}_\sigma^2 - \frac{d_4}{16} \sum_{\nu \neq \mu} \hat{k}_\nu^4, \quad (14)$$

and

$$G_{\nu,\mu}(k) = \frac{\hat{k}_\mu \hat{k}_\nu}{4} \tilde{G}_{\nu,\mu}(k) \quad (15)$$

$$\tilde{G}_{\nu,\mu}(k) = d_1 - d_2 \frac{(\hat{k}_\rho^2 + \hat{k}_\sigma^2)}{8} + d_3 \frac{\hat{k}_\rho^2 \hat{k}_\sigma^2}{12} + d_4 \frac{\hat{k}_\nu^2}{4}, \quad (16)$$

where all indices (μ, ν, ρ, σ) are different.

The coefficients d_{1-4} distinguish the different choices of links:

1. Fat-7 links:

$$d_1 = 1, \quad d_2 = 1, \quad d_3 = 1, \quad d_4 = 0. \quad (17)$$

2. $O(a^2)$ improved links:

$$d_1 = 0, \quad d_2 = 1, \quad d_3 = 1, \quad d_4 = 1. \quad (18)$$

3. HYP smeared links:

$$d_1 = (2/3)\alpha_1(1 + \alpha_2(1 + \alpha_3)), \quad d_2 = (4/3)\alpha_1\alpha_2(1 + 2\alpha_3), \quad d_3 = 8\alpha_1\alpha_2\alpha_3, \quad d_4 = 0. \quad (19)$$

There are two interesting choices for the α_i . The first was determined in Ref. [6] using a non-perturbative optimization procedure: $\alpha_1 = 0.75$, $\alpha_2 = 0.6$, $\alpha_3 = 0.3$. The second is chosen so to remove $O(a^2)$ flavor-symmetry breaking couplings at tree level. This gives the same d_i as for Fat-7 links.

B. Static Potential

With the gluon propagator we can immediately compute the static Coulomb potential,

$$V_c(r) = \int_{ak} \exp(i\vec{k} \cdot r) G_{00}(q_\mu = (0, \vec{k})) \quad (20)$$

where $\int_{ak} = \prod_j \int_{-\pi}^{\pi} d(ak_j)/(2\pi)$ will be the symbol for integration over the (rescaled) momentum hypercube. With our conventions, the continuum potential is $V(r) = 1/(4\pi r)$, and so plotting the rescaled lattice potential $4\pi r V(r)$ immediately exposes the lattice artifacts of a particular action. We show results for this quantity in Fig. 1 for the four candidate actions of our study. The tree level Symanzik action has no $O(a^2)$ nor $O(a^4)$ discretization errors and also has the smallest scaling violations. The other actions have $O(a^4)$ scaling violations, which should be of opposite sign for the Wilson action versus the Iwasaki and DWB2 actions. This is seen in the figure. However, the most noticeable feature of the potential is the systematic distortion of $4\pi r V(r)$ below unity at small lattice distance as the coefficient c_1 becomes more negative. The results of this calculation strongly disfavor use of a large negative value of c_1 for any lattice simulations with physics related to the short distance part of the potential.

The potential itself is, of course, unaffected by any fattening of the fermion's gauge connection, but we can also define a "smeared potential," in which the gluon propagator G_{00} is replaced by \mathcal{G}_{00} . This quantity has the physical interpretation of the potential seen by a heavy lattice quark whose gauge connection is a fat link. Results for two gauge actions (Wilson and tree level Symanzik) and two smearings, HYP and Asqtad, are shown in Fig. 2.

Both of these smearings distort the lattice potential at small r/a . The immediate conclusion that one draws from these pictures is that one should not do simulations involving heavy quarks with smeared links – the loss of Coulomb

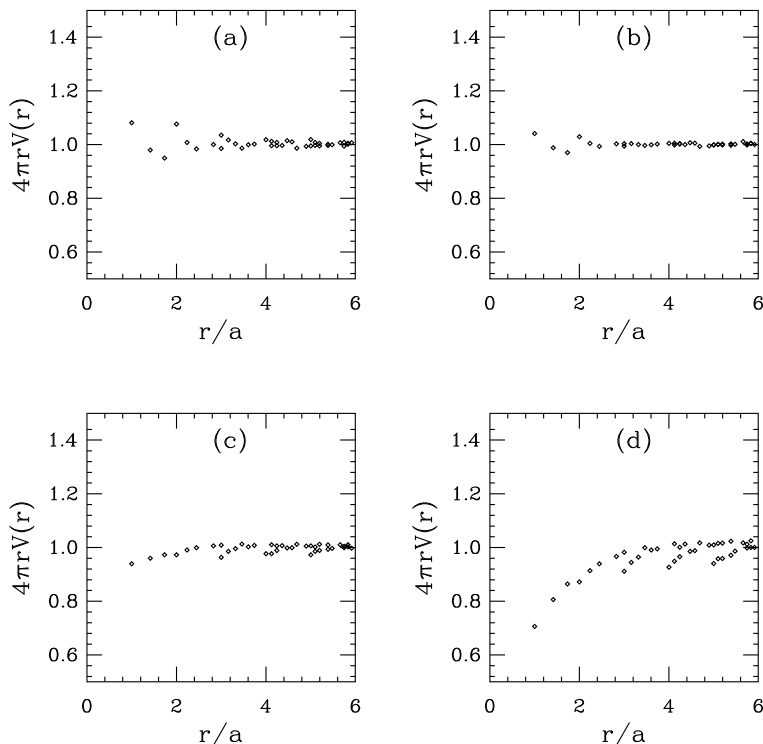


Figure 1: The scaled static potential $4\pi rV(r)$ for several lattice actions: (a) Wilson ($c_1 = 0$), (b) tree level Symanzik ($c_1 = -1/12$), (c) Iwasaki ($c_1 = -0.331$)(d) DWB2 ($c_1 = -1.4088$).

behavior at short distance will allow the wave function of a heavy quark-antiquark bound state to spread out, the value of the wave function at the origin will be small, and hyperfine splittings will collapse. This effect is readily seen in simulations.

A particular example of the danger of fattening heavy quarks is seen in the recent MILC study of heavy quark-light quark decay constants, f_D and f_B [19]. One of the data sets collected by these authors used fermions fattened with a large amount of APE-smearing [20] ($c = 0.45$, $N = 10$ in the conventions of Ref. [18]). This amount of smearing produces a noticeable suppression of the static potential out to $r/a \simeq 3 - 4$. The authors observed a twenty per cent reduction in f_B . This effect presumably would go away at smaller lattice spacing, but comparing Fig. 2, one would need to halve the lattice spacing to reduce the lattice artifact to the level of HYP blocking.

However, the motivation for using smeared links in a fermion action is, by and large, to improve the chiral properties of the action. This is physics applicable to light quarks, not heavy ones. Many simulations of light quarks with various degrees of fattening show no ill effects on spectroscopy or on matrix elements – generally, improvement of scaling is observed [1, 2]. Fattening is something which can be done selectively, in a mass-dependent way. Altering the gauge action will affect quarks regardless of their mass.

Finally, we call the reader's attention to the rather large lattice spacing artifacts of the Asqtad-smearred potential as compared to the HYP- smearred potential (or any of the usual unsmeared potentials).

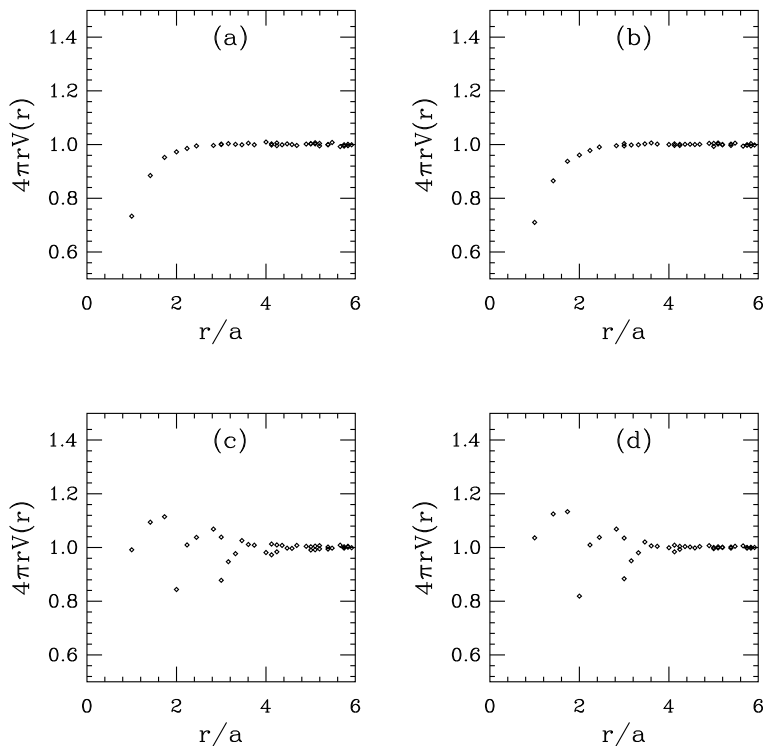


Figure 2: The scaled static “smeared potential” $4\pi rV(r)$ for two lattice actions and two smearing functions: (a) Wilson ($c_1 = 0$) gauge action with HYP blocking, (b) tree level Symanzik ($c_1 = -1/12$) gauge action with HYP blocking, (c) Wilson ($c_1 = 0$) gauge action with Asqtad blocking, (d) tree level Symanzik ($c_1 = -1/12$) gauge action with Asqtad blocking,

C. One-loop Perturbative Matching Factors

A matrix element of an observable computed using one regularization (\overline{MS}) is related in perturbation theory to a linear combination of observables computed using another (lattice) regularization through a matrix of matching coefficients Z_{nm}

$$\langle f|O_n^{cont}(\mu)|i\rangle_{\overline{MS}} = a^D \sum_m Z(\mu, a)_{nm} \langle f|O^{latt}(a)_m|i\rangle \quad (21)$$

where each coefficient is a difference between (the finite part of a) continuum-regulated and a lattice-regulated expression

$$Z_{nm}(\mu, a, m) = 1 + \frac{g^2}{16\pi^2} (\Delta_{\overline{MS}}^F - \Delta_{latt}). \quad (22)$$

(g^2 is the squared coupling). For currents, it is customary to divide out the quadratic Casimir C_F and to present results for $z = (\Delta_{\overline{MS}}^F - \Delta_{latt})/C_F$. For four-quark operators (for weak-interaction matrix elements, for example), it is customary just to write $b = \Delta_{\overline{MS}}^F - \Delta_{latt}$. Generally, in the context of perturbation theory, one attempts to design actions, operators, and methods of performing perturbative calculations [21] so that the z or b coefficients are

	Wilson	Tree level Sym	Iwasaki	DWB2
Z_V	-15.33	-11.91	-7.44	-3.03
Z_A	-13.79	-10.72	-6.71	-2.75
Z_S	-19.31	-15/08	-8.90	-1.04
Z_P	-22.38	-17.47	-10.36	-1.59
Z_+	-36.63	-28.86	-19.15	-1.08
Z_-	-43.20	-32.78	-18.27	-1.61

Table I: z and b coefficients for one loop matching factors for some two- and four-fermion operators, for thin-link clover fermions with $C_{SW} = 1$, and gauge action as labelled. Errors are ± 1 in the last digit shown.

	Wilson	Tree level Sym	Iwasaki	DWB2
Z_V, Z_A	-14.80	-11.24	-6.76	-2.63
Z_P, Z_S	-39.24	-30.35	-17.99	-4.38
Z_+	-25.18	-19.25	-12.54	-7.86
Z_-	-68.06	-51.45	-29.0	-5.35

Table II: z and b coefficients for one loop matching factors for some two- and four-fermion operators, for naive fermions with $C_{SW} = 1$, and gauge action as labelled. Errors are ± 1 in the last digit shown.

minimized. The reader might recall that at typical lattice spacings studied today, typical choices for $g^2/4\pi$ range from 0.1-0.2, so a z or b of about 20 implies a twenty to forty per cent effect from a one loop calculation—perhaps a bit large for comfort. Typically, with fat links one can reduce these numbers by an order of magnitude, as seen by perturbative calculations[18, 22, 23] or nonperturbative simulation [24].

We have computed one loop perturbative matching factors for local currents $\bar{\psi}(x)\Gamma\psi(x)$ —for the vector (V), axial vector (A), scalar (S) and pseudoscalar (P) currents, as well as the matching factors for the four-fermion operators $O_{\pm} = O_1 \pm O_2$, built from

$$O = (\bar{q}_{\alpha}^{(1)}\Gamma_1 q_{\beta}^{(2)}) \otimes (\bar{q}_{\gamma}^{(3)}\Gamma_2 \hat{q}_{\delta}^{(4)}). \quad (23)$$

where $\Gamma_1 = \Gamma_2 = \gamma_{\mu}(1 - \gamma_5)$. $O_{\pm} = O_1 \pm O_2$; if color labels $\alpha = \delta, \beta = \gamma$, $O = O_1$; if color labels $\alpha = \beta, \gamma = \delta$, $O = O_2$. (These operators have no penguin contributions.)

An important indicator of chiral improvement [25] for nonchiral actions is the difference $z_V - z_A = (z_P - z_S)/2$: the mixing of four-fermion operators into the opposite chirality sector is controlled by this quantity.

Our results are shown in Tables I, II. For operators with anomalous dimensions (all but the vector and axial vector currents) our results are for the case (lattice spacing $a \times$ regularization point μ) = 1. We see that as c_1 becomes increasingly negative, the z and b coefficients generally shrink.

We next repeat these calculations, but now with fermions with HYP-smearred gauge connections. Tables III, IV show a dramatic reduction in the z and b coefficients, even when the Wilson gauge action is used. With the reduction of these numbers comes also a reduction in the difference $z_V - z_A$ for clover fermions.

From the point of perturbative theory for matching factors, the conclusion is clear: it is much more efficient to fatten the fermion gauge connections than to increase c_1 in the gauge action.

	Wilson	Tree level Sym	Iwasaki	DWB2
Z_V	-1.38	-1.18	-0.89	-0.50
Z_A	-1.30	-1.11	-0.84	-0.48
Z_P	0.04	0.54	1.55	3.77
Z_S	-0.12	0.41	1.45	3.72
Z_+	-6.43	-6.14	-5.89	-6.12
Z_-	2.16	3.11	4.84	8.34

Table III: z and b coefficients for one loop matching factors for some two- and four-fermion operators, for clover fermions with $C_{SW} = 1$, HYP-smearred links, and gauge action as labelled. Errors are ± 1 in the last digit shown.

	Wilson	Tree level Sym	Iwasaki	DWB2
Z_V, Z_A	-0.95	-0.79	-0.59	-0.33
Z_P, Z_S	-0.62	-0.01	1.20	3.61
Z_+	-4.75	-4.65	-4.75	-5.53
Z_-	1.92	2.95	4.81	8.37

Table IV: z and b coefficients for one loop matching factors for some two- and four-fermion operators, for naive fermions with $C_{SW} = 1$, HYP-smearred links, and gauge action as labelled. Errors are ± 1 in the last digit shown.

D. On-shell Scattering Amplitudes

Let us recall that the motivation for introducing smeared links into staggered fermions was to suppress the coupling between the region of the fermion Brillouin zone near $k_\mu = (0, 0, 0, 0)$ and regions of the Brillouin zone corresponding to doublers: one or more $k_\mu \simeq \pi$. Smearing amounts to a form factor which suppresses the emission or absorption of gluons whose exchange could scatter a quark from a $k_\mu \simeq 0$ into a doubler state. The absence of this kind of scattering means an improvement in flavor symmetry for staggered fermions since a process which transforms a quark of one flavor (living in one part of the Brillouin zone) into another flavor is reduced.

To quantify this scenario, let's imagine (in the continuum, first) the scattering of two on-shell quarks of momentum $\pm p_1$ into two quarks of momentum $\pm p_2$. The T -matrix for the scattering is

$$T(k) = [\bar{u}(p_2)\gamma_\mu u(p_1)]G_{\mu\nu}(k)[\bar{u}(-p_2)\gamma_\nu u(-p_1)] \quad (24)$$

where of course $k = p_1 - p_2$. Imposing the on-shell constraint $\gamma \cdot p|u(p_i) = 0$, we see that the gauge-dependent term (proportional to $(\xi - 1)k_\mu k_\nu / k^2$) vanishes, leaving the scattering amplitude proportional to the Feynman gauge gluon propagator (and spinor factors). The reader can quickly confirm that the same result obtains for naive fermions and the Wilson gluon propagator.

Now recall that the effect of smearing is to replace the gluon propagator by the ‘‘smeared gluon propagator,’’ Eq. 12. As a way of comparing the level of flavor symmetry violation, we just look at the Feynman gauge propagator (appropriate for flavor symmetry restoration with thin link fermions) or the smeared propagator. We plot $k^2 \sum_\mu G_{\mu\mu}$ versus $\sqrt{k^2}$ for a set of momenta $k_\mu = \pi n_\mu / 8$, $n_\mu = 1 \dots 8$. Fig. 3 shows our results for thin link actions. As c_1 becomes more negative, the ‘‘scattering amplitude’’ at large k decreases. We would anticipate that flavor symmetry would be improved by negative c_1 . We will confirm this expectation in Sec. 6.

However, much greater suppression at large k is achieved by converting to a smeared link. In Fig. 4 we show several examples of $k^2 \sum_\mu G_{\mu\mu}$, which parameterizes the scattering of smeared link fermions. HYP links and the Wilson gauge action produce more suppression than thin links and the DWB2 action. Clearly, a combination of greater c_1 and a

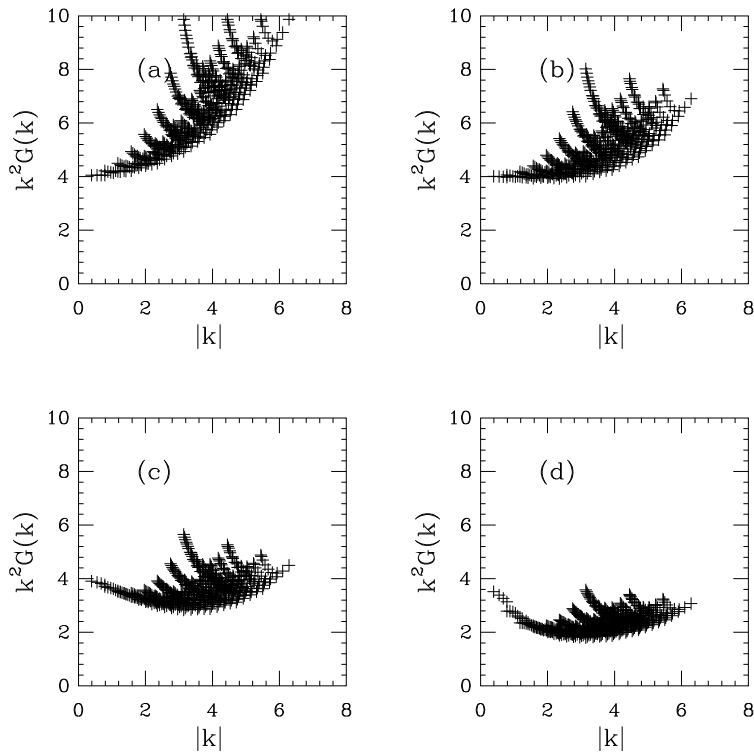


Figure 3: $k^2 G_{\mu\mu}(k)$ for several lattice actions: (a) Wilson ($c_1 = 0$), (b) tree level Symanzik ($c_1 = -1/12$), (c) Iwasaki ($c_1 = -0.331$)(d) DWB2 ($c_1 = -1.4088$).

smearing link would produce a larger effect.

There is an obvious qualitative connection between Figs. 3 and 4 and the results of one-loop perturbation theory for matching coefficients: As the magnitude of the gluon propagator shrinks at large k , so does its contribution to the integrals of the perturbative calculation.

IV. THE NON-PERTURBATIVE STATIC POTENTIAL

We start our discussion of the non-perturbative properties of the different actions with the static quark potential. The perturbative results of Sect. 3.2 suggest that the thin link Symanzik action has the smallest lattice distortion. The Wilson action has a positive lattice correction at small distance and observable rotational symmetry breaking even at $r/a = 2 - 3$. The perturbative DBW2 potential has a larger and negative correction at $r/a = 1$ and observable rotational symmetry breaking even at $r/a = 4 - 5$. The perturbative HYP smeared Wilson gauge action potential has similar distortion at $r/a = 1$ as the DBW2 but much smaller rotational symmetry violation while the Asqtad smeared Wilson gauge potential has smaller distortion at short distances but larger rotational symmetry violation.

We studied the non-perturbative static potential on Wilson, 1-loop Symanzik and DBW2 gauge backgrounds with and without HYP smearing. The simulations were carried out on $8^3 \times 24$ lattices with Sommer scale $r_0/a \sim 3.0$ for all three actions, at $\beta = 5.7$ for Wilson, $\beta = 7.775$ for Symanzik and $\beta = 0.82426$ for the DBW2 action. At large

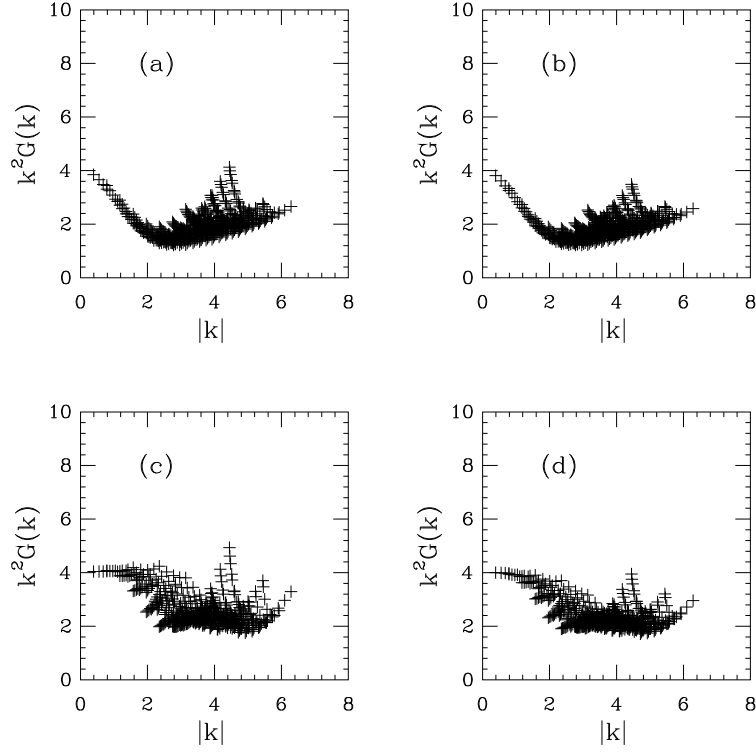


Figure 4: $k^2 \mathcal{G}_{\mu\mu}(k)$ for two lattice actions and two smearing functions: (a) Wilson ($c_1 = 0$) gauge action with HYP blocking, (b) tree level Symanzik ($c_1 = -1/12$) gauge action with HYP blocking, (c) Wilson ($c_1 = 0$) gauge action with Asqtad blocking, (d) tree level Symanzik ($c_1 = -1/12$) gauge action with Asqtad blocking,

distances the smeared and thin link potentials differ only by an irrelevant additive constant. In Fig. 5 we plot both the smeared and thin link potentials, the former one shifted by a constant to match the thin link potential at $r/a = \sqrt{7}$, a somewhat arbitrarily chosen matching point. We fit each potential following the method proposed in [26] and used with the HYP potential in [27, 28] taking a four parameter functional form

$$V_{\text{latt}}(r) = V_{\text{cont}}(r) + \epsilon(V_c(r) - \frac{1}{4\pi r})$$

where V_{cont} is the continuum potential

$$V_{\text{cont}} = -\frac{e}{r} + V_0 + \sigma r,$$

and $V_c(r)$ is the lattice Coulomb potential of Eq. 20. The term $\epsilon(V_c(r) - 1/(4\pi r))$ is an attempt to model and remove the lattice artifacts of the potential. It is difficult to judge how much of the lattice artifacts can be described by this term, only the quality of the fit can justify its use.

Fig. 5a shows the Wilson gauge action potential measured with thin links (diamonds) and with HYP links (octagons). The dotted line of the figure correspond to the fit of the continuum potential V_{cont} after the removal of the lattice artifacts while the dashed line is the same continuum potential obtained with the HYP smeared links and their corresponding perturbative corrections. The fact that it is impossible to resolve the two different lines in

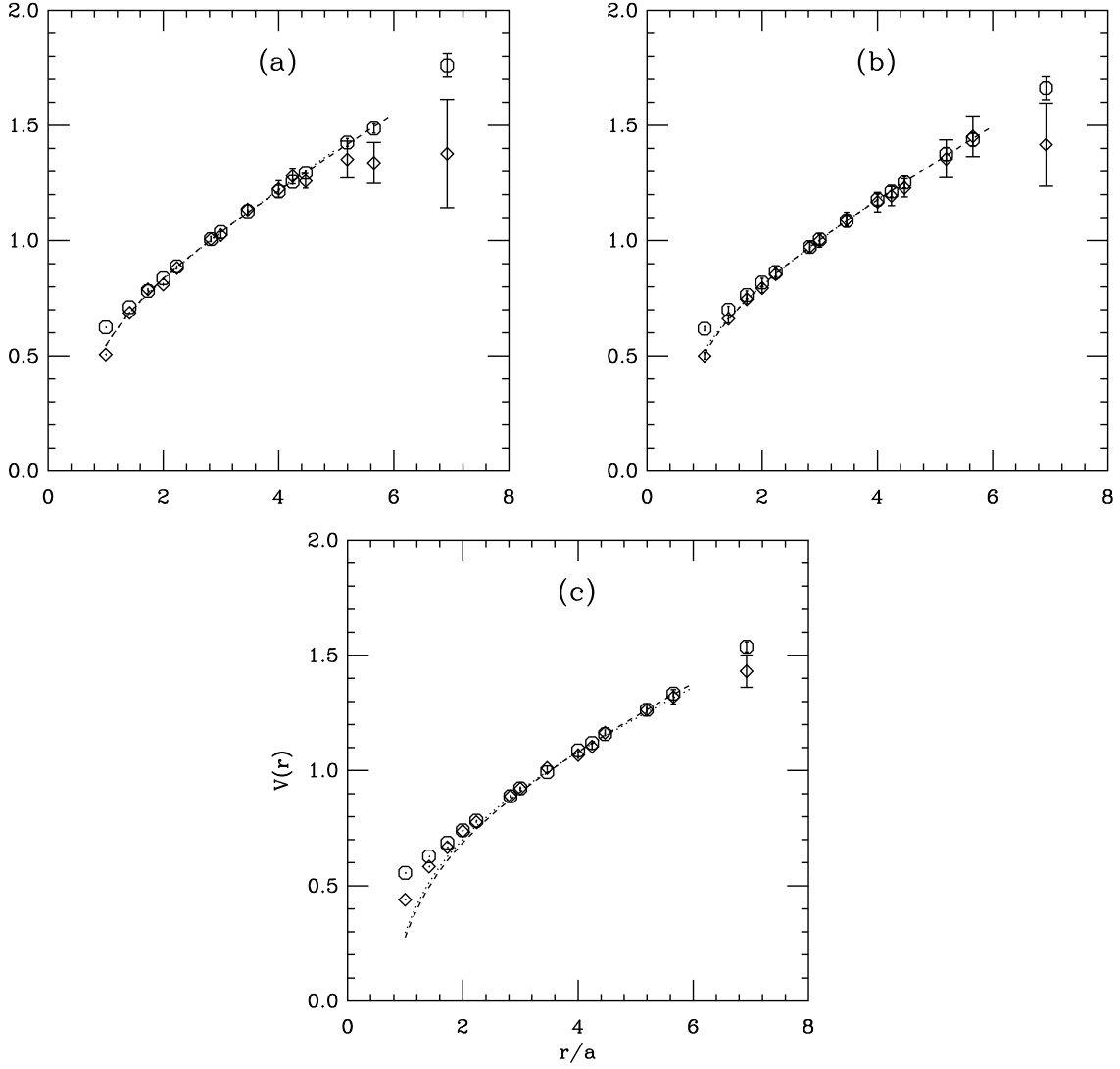


Figure 5: The static potential measured with a) Wilson gauge action, b) 1-loop Symanzik gauge action and c) DBW2 gauge action. In all cases both the thin link (diamonds) and HYP smeared (octagons) potentials are plotted, shifted to agree at $r/a = \sqrt{7}$. The dotted and dashed lines are the fitted continuum potentials as described in the text.

the figure indicates that the lattice artifacts are consistently removed. Also, the sign and relative magnitude of the lattice corrections are what we expected from the perturbative Coulomb potential. Fig. 5b is the same for the 1-loop Symanzik action. The smeared and thin link results are consistent, indistinguishable. The thin link potential has very small lattice artifacts but after removing the lattice correction both thin and HYP potentials predict the same continuum values. In Fig. 5c we plot the corresponding potential data for the DBW2 action. The agreement between the thin and HYP smeared potentials is good though not as perfect as in the previous two cases, mainly because of the stronger rotational symmetry violation of the thin link potential. The results agree with the perturbative predictions:

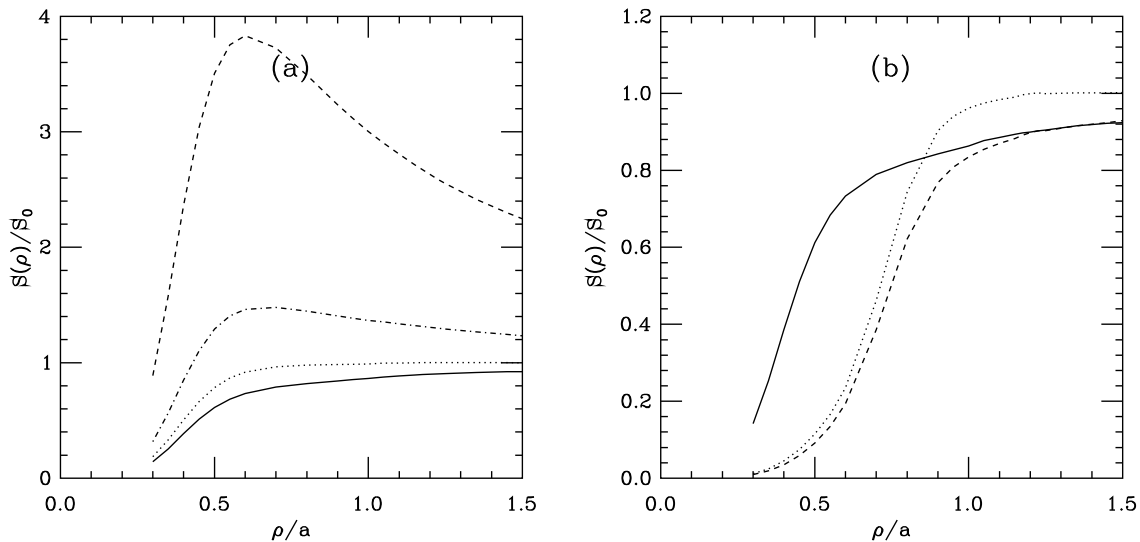


Figure 6: The action of smooth instantons, normalized by the continuum value, as the function of the instanton radius, calculated with different actions. a) solid line: Wilson action, dotted line: tree level Symanzik action; dashed-dotted line: Iwasaki action; dashed line: DBW2 action. b) solid line: Wilson action (thin link); dashed line: HYP smeared Wilson action; dotted line: HYP smeared tree level Symanzik action.

even the thin link DBW2 potential has a large distortion at $r/a = 1$, about the same as the HYP link potential with Wilson or 1-loop Symanzik action. If the value of the potential (or any other quantity) is important at $r/a = 1$, the DBW2 action is not a good choice to use.

It is difficult, if not impossible, to prove how the lattice Coulomb term could describe the lattice artifacts of the non-perturbative potential. Only the fact that the different potential measurements with thin and HYP links give consistent continuum results for all three gauge actions justifies its use.

Recent calculations of the static potential with the DBW2 action did not show such a large distortion at small distances. However in Ref. [29] only the on-axis potential was measured at distances $r/a \geq 2$. From that data it would have been hard to see the distortion at small distances.

V. TOPOLOGY AND THE GAUGE ACTION

A. Smooth instantons

It is generally believed that flavor symmetry violation for staggered fermions, the residual chiral symmetry violation of domain wall fermions, and the computationally most demanding small eigenmodes of the overlap fermions are due to small scale, plaquette level vacuum fluctuations. Smearing attempts to remove these objects by averaging the gauge links while the Iwasaki and DBW2 actions do the same by making it energetically unfavorable to create them in the first place. That mechanism can be seen clearly from the action of smooth instantons. We calculated the instanton action on a set of smooth instantons with varying radii. These instantons were created in singular gauge on 32^4 lattices and blocked twice in order to approximate the smooth, continuum solution. In Fig. 6a we show the result, normalized by the continuum instanton action, for Wilson, tree level Symanzik, Iwasaki and DBW2 actions. A

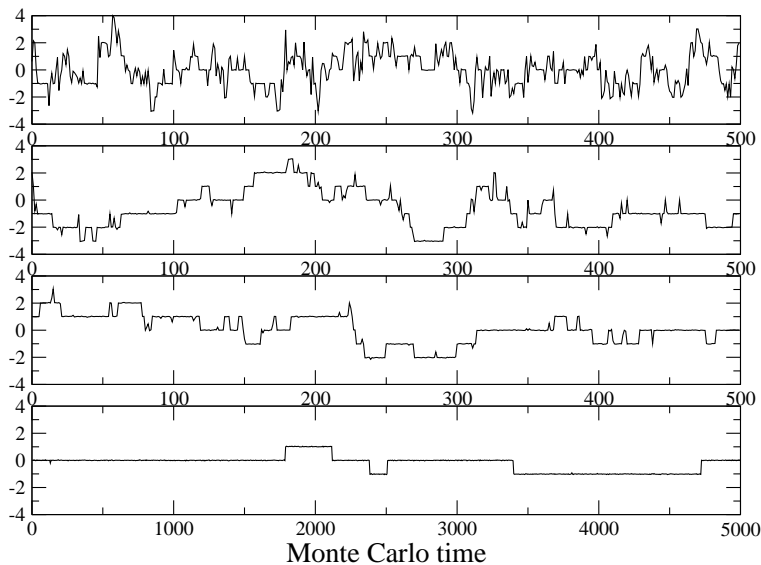


Figure 7: The Monte Carlo time history of the topological charge with various gauge actions. The actions are (from top to bottom) Wilson ($\beta = 6.0$), Symanzik ($\beta = 8.4$), Iwasaki ($\beta = 2.6$) and DBW2 ($\beta = 1.04$).

perfect lattice action should have a profile that is less than one for small radii and one for radii larger than a critical value where the vacuum fluctuation becomes an instanton. At the critical radius the action function is non-analytic, it develops a kink. None of our actions can reproduce this behavior, but not surprisingly the closest to it is the tree level Symanzik action. The Wilson action profile approaches the continuum value more slowly, from below. The Iwasaki action overshoots the continuum value by about 50% at $r/a \sim 0.6$, suppressing fluctuations of this size. The corresponding DBW2 curve is nothing less than shocking. The curve rises to almost four at $r/a \sim 0.6$ and even at distance $r/a = 1.5$ it is above two. The DBW2 action strongly suppresses instantons and dislocations with radius $0.3 < r/a < 2-3$. The very small fluctuations are still present, but small radius instantons are disfavored. On lattices where these small instantons are important physically one would expect fairly large lattice artifacts from the DBW2 action.

Smearing attempts to remove dislocations seen by the fermions by averaging the gauge links. Fig. 6b compares the HYP smeared instanton profiles of the Wilson and Symanzik actions. For reference we include the thin link Wilson action profile again. The most important conclusion from Fig. 6b is that smearing removes dislocations with radius $r/a < 0.5$, the action profile rises only at $r/a \sim 0.7$. Even though the gauge configuration can have plenty of small instantons and dislocations, most of these are not seen by the fermions.

B. The autocorrelation of the topological charge

We have seen that as the coefficient c_1 in the action becomes more negative, the action favors small instantons less and less. In a Monte Carlo simulation with local (one-link) updates, change of topology always occurs through the (dis)appearance of small topological objects. It is thus not very surprising that the suppression of small topological objects implies that topology changes less often. In Fig. 7 we show the Monte Carlo time history of the topological charge with different gauge actions. The charge was measured using the RG improved charge operator [30, 31] after

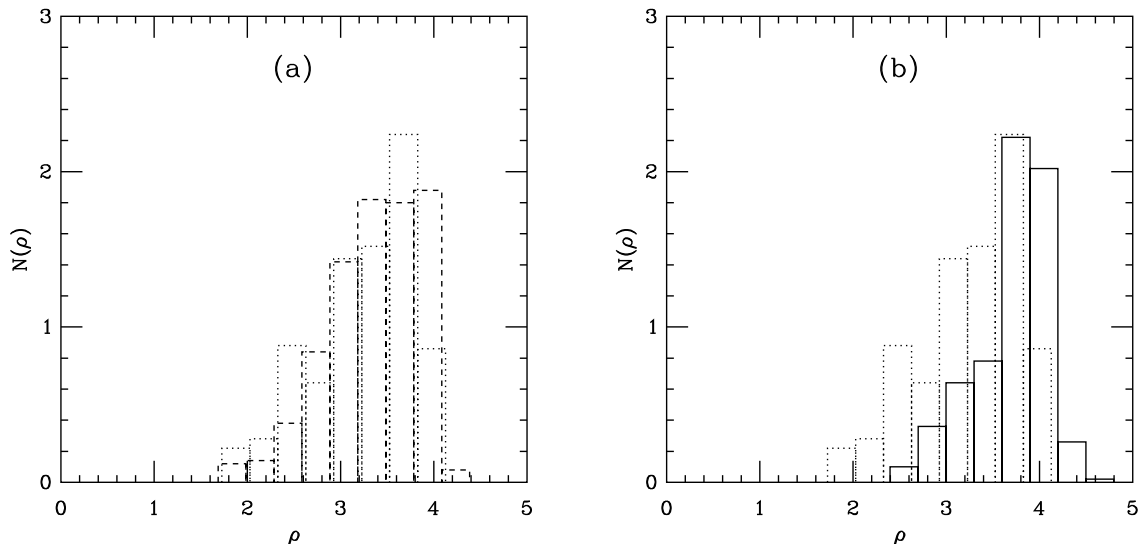


Figure 8: Instanton size distribution of the different actions after two HYP smearing steps. a) Wilson (dotted lines) and Iwasaki (dashed lines) actions; b) Wilson (dotted lines) and DBW2 (solid lines) actions.

8 levels of APE smearing steps. The units on the horizontal axis correspond to ten full sweeps of a combination of one overrelaxation and one Metropolis step over the whole lattice. The lattice size in these simulations was 12^4 in all cases and the β values were matched to correspond to the same lattice spacing, $a = 0.095$ fm, set by the Sommer scale. Indeed, the difference among the gauge actions is striking. Notice that for the DBW2 action the MC time scale is an order of magnitude different. The integrated autocorrelation time of the topological charge was estimated to be 100 and 700 sweeps for the Wilson and the Iwasaki action respectively. In the case of the DBW2 action the autocorrelation time is so enormous that the available data was not enough even to estimate it. It is also interesting to observe that the plaquette autocorrelation time is 10, 7 and 5.5 for the Wilson, Iwasaki and the DBW2 action. The very large autocorrelation time of the topological charge of the DBW2 action was also noted by the RBC collaboration [4].

It is also noticeable that as c_1 becomes more negative, and the change between topological sectors occurs less frequently, the charge also becomes closer on the average to integer values. This also indicates the strong suppression of small instantons and in general the suppression of gauge configurations close to the boundary between two charge sectors.

C. The instanton size distribution

The instanton action profiles of Fig. 6 indicate a slight suppression of small instantons for the Iwasaki action, and strong suppression of small and even larger instantons for the DBW2 action. On configurations with $a \sim 0.095$ fm the average instanton radius is about $r/a = 3$ but smaller instantons should be also present. In order to see if the different gauge actions have different instanton size distributions we have measured instanton sizes on a set of $a \sim 0.095$ fm configurations. We measured the topological charge density after 2-4 levels of HYP smearing [32] and compared it to smooth instanton profiles. This is the same method we used in Ref. [30, 31] except we do not extrapolate the instanton size to zero smearing level. In Fig. 8 we compare the instanton size distribution of the different actions after

two HYP smearing steps. We have used the same 12^4 , $a = 0.095$ fm configurations we analyzed in the previous section and normalized the distribution by the number of configurations. As Fig. 8a illustrates, there is not much difference between the Wilson and Iwasaki actions. The size distribution peaks around $\rho/a = 3.5$ and both actions predict the same topological density. (We are not concerned about the physical significance of the topological density here. Since we have used the same lattice spacing and analysis method with both configuration sets, comparing the two densities gives information about the two actions.) In contrast, the Wilson and DBW2 actions differ significantly, as Fig. 8b illustrates. The smaller instantons are suppressed by the DBW2 action, and the topological density is about 30% less on the DBW2 than on the Wilson configurations. If we consider the physical picture of quark propagation, where the quarks hop from instanton to anti-instanton in the vacuum [33], lack of instantons could point to observable scaling violations in the light hadron spectrum.

VI. FLAVOR SYMMETRY VIOLATION IN STAGGERED ACTIONS

Smearred actions are used with staggered fermions because they considerably reduce flavor symmetry violations. Both the Asqtad and HYP smearing are $O(a^2)$ perturbative improved though the coefficients of the HYP smearing are non-perturbatively optimized. Relative to the thin link staggered action, Asqtad fermions improve flavor symmetry by a factor of five, HYP fermions by about a factor of ten. Based on our perturbative and instanton analyzes, flavor symmetry could also be improved by modifying the gauge action. At first this approach might look attractive: it is much easier to simulate thin link fermions with a complicated gauge action than smeared link fermions. However taking the easy way might have serious consequences later on. The potential data indicates that the DBW2 action distorts short distance behavior, the time evolution of the topological charge points to unacceptably long autocorrelation times, the low topological density could imply large lattice artifacts. Nevertheless, in this section we consider the possibility of using different gauge actions with and without smearing in staggered fermion simulations and investigate the level of flavor symmetry violation these actions show.

We have studied the quenched staggered spectrum on our $8^3 \times 24$, $r_0/a \sim 3.0$, $a \sim 0.17$ fm configurations. Before presenting our results for the spectrum, first we look at the distribution of the plaquette on these configurations. In [6] it was argued and illustrated that the end tail of the plaquette distribution is correlated with flavor symmetry breaking of staggered fermions. The argument is quite simple: flavor symmetry violation is caused by the strongly fluctuating gauge fields at the hypercubic level. These gauge links create plaquettes with very small value, therefore the number of plaquettes with very small value indicate the level of flavor symmetry breaking the fermions observe.

In Fig. 9 we show the tail of the plaquette distribution, normalized by the number of configurations for the Wilson, 1-loop Symanzik and DBW2 gauge actions. Fig. 9a compares the plaquettes constructed from thin links. Not surprisingly, the DBW2 action is a factor of eight better than the Wilson action. The 1-loop Symanzik action is also better than the Wilson action by about a factor of two. In Fig. 9b we plot the plaquette distribution of the Wilson and 1-loop Symanzik actions after one level of HYP blocking. The latter is again a factor of two better than the former, but both are an order of magnitude better than the thin link DBW2 action. (Observe the scale difference of the two figures.) Does the implication from the tail of the plaquette agree with the actual flavor symmetry violation of the different actions? We use the parameter

$$\Delta_\pi = \frac{m_\pi - m_G}{m_G}, \quad (25)$$

which measures the relative difference between the Goldstone pion mass and the non-Goldstone pions, to compare the different actions. This quantity diverges at zero quark masses and depends strongly on the lattice spacing, but since we have done all the simulations at approximately identical lattice spacings and volumes, Δ_π as a function of the Goldstone particle, is a good indicator of the flavor symmetry violation of the different actions. The results, shown in Fig. 10, confirms these expectations. The thin link 1-loop Symanzik action improves flavor symmetry relative to the Wilson action by about 30%. The thin DBW2 action is even better, it has flavor symmetry violation at the level

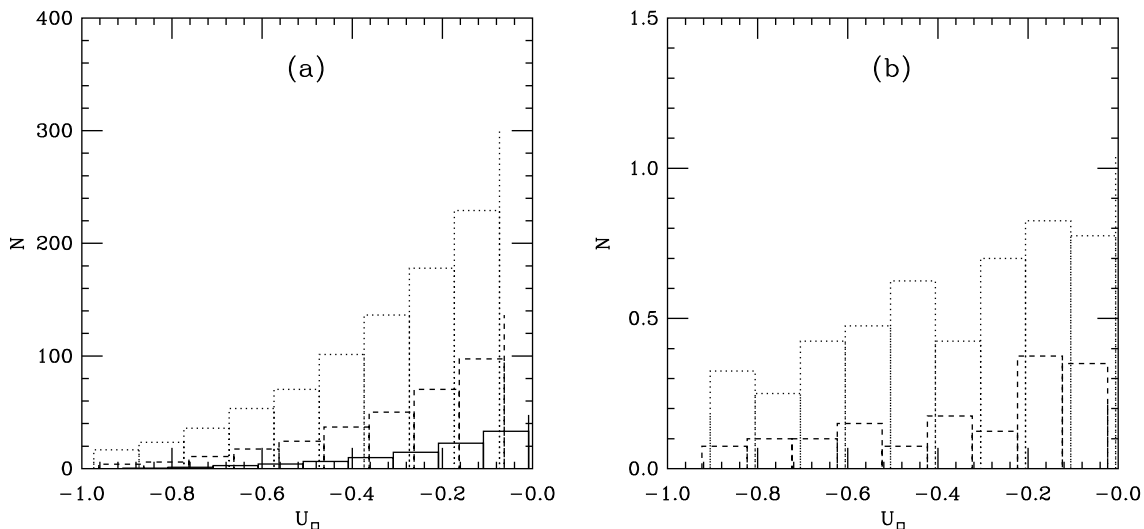


Figure 9: The tail of the plaquette distribution for different gauge actions a) with thin links and b) after HYP smearing. Dotted line: Wilson, dashed line: 1-loop Symanzik, solid line: DBW2 action. Observe the scale difference of the two figures.

of the Asqtad smeared Wilson action. HYP smearing, even on Wilson configurations, is a factor of two better. One can reduce flavor symmetry violation even further by using the 1-loop Symanzik action. It is not easy to see from the figure, but 1-loop Symanzik is about 30% better than Wilson, even after HYP smearing. Since the Symanzik action has better scaling properties than the Wilson action and does not suffer from topological autocorrelation slow down like the DBW2 and Iwasaki actions do, a HYP smeared Symanzik action appears to be the best choice for staggered simulations.

VII. SMEARING, IMPROVED ACTIONS AND THE OVERLAP OPERATOR

A. Fermionic charge and overlap

Since a large negative c_1 suppresses the creation of small instantons or other objects where the gauge field is on the boundary between different topological sectors, gauge actions with a more negative c_1 result in smaller residual masses in domain wall simulations. A similar mechanism is at work in the case of the overlap. The overlap operator is defined in terms of a simple Dirac operator (e.g. Wilson) D_0 by the formula

$$D_{ov} = 1 - A [A^\dagger A]^{-\frac{1}{2}}, \quad A = 1 + s - D_0, \quad (26)$$

where s is a real parameter. If the gauge configuration is close to the boundary between different topological sectors, $A^\dagger A$ has to have a small eigenvalue. Therefore, the suppression of these boundary gauge configurations can also thin out the small eigenvalues of $A^\dagger A$. This is important for practical applications since the cost of the overlap is governed by the condition number of $A^\dagger A$. Assuming for instance that Chebyshev polynomials are used to approximate the inverse square root, the order of the Chebyshev polynomial is inversely proportional to the square root of the smallest eigenvalue where the Chebyshev approximation has to work. In Table V we show the average smallest and eighth smallest eigenvalue of $A^\dagger A$ with D_0 being the Wilson Dirac operator, on different sets of gauge backgrounds with the

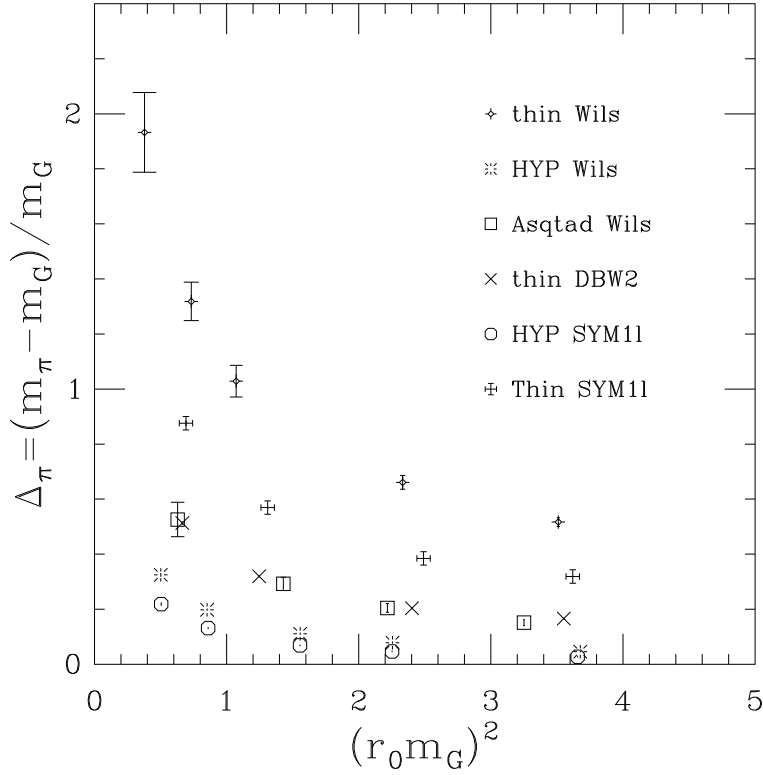


Figure 10: Flavor symmetry violation of staggered fermions on different gauge action backgrounds with different smearing transformations. All data on this plot is from quenched simulations with lattice spacing $a \simeq 0.17\text{fm}$.

same lattice spacing. The lattice size was 12^4 and the β values were 6.0 (Wilson), 2.60 (Iwasaki), 8.40 (Symanzik) and 1.04 (DBW2) and each set contained 50 independent configurations. For this qualitative test we fixed the value of s to be 0.5, except on the HYP smeared configurations, where it was set to zero. Although in principle s would have to be optimized for each type of gauge background separately, we chose to fix it close to the overall optimal value. This is sufficient for our purposes, moreover, an optimization for the smallest eigenvalues of $A^\dagger A$ and for locality would yield different values.

There is a clear trend that a more negative value of c_1 pushes up the smallest eigenvalues. However, the reader's attention is called to the last entry in the table, where we have HYP-smeared the links in the fermion action and retained the Symanzik gauge action. The gain in time for simulating this action is almost a factor of two better than for the DBW2 action.

Generally, overlap simulations are accelerated by projecting out (and treating exactly) the eigenvectors corresponding to the smallest few eigenvectors. This results in a gain of about a factor of 2 for the Wilson action, and smaller factors for the other actions studied. To facilitate a comparison we also included in the table the factor one can gain in speed compared to Wilson gauge action without projecting out any eigenvector.

A major difference between the overlap and domain wall formulation is that for the overlap small eigenvalues of $A^\dagger A$ are only a nuisance, as they make the calculation more expensive. On the other hand, in domain wall simulations the extension of the lattice in the fifth direction is fixed and this results in different chirality violations and residual mass effects configuration by configuration. This is the main reason why improvement of the gauge action was so badly

Action	$\langle \lambda_1 \rangle$	t_{W1}/t	$\langle \lambda_8 \rangle$	t_{W1}/t
Wilson	0.013(2)	1.0	0.061(1)	2.17
Symanzik	0.044(4)	1.84	0.105(1)	2.84
Iwasaki	0.065(4)	2.24	0.130(1)	3.16
DBW2	0.160(5)	3.51	0.217(1)	4.09
Symanzik+HYP	0.46(3)	5.95	0.737(2)	7.52

Table V: The average smallest eigenvalue (λ_1) and the 8th smallest eigenvalue (λ_8) of $A^\dagger A$ and the factor of CPU time reduction compared to the Wilson action with no eigenvector projected out. The first two columns refer to the case when no eigenvalues are projected out, the last two columns to the one when the eight lowest eigenvectors are projected out and treated exactly.

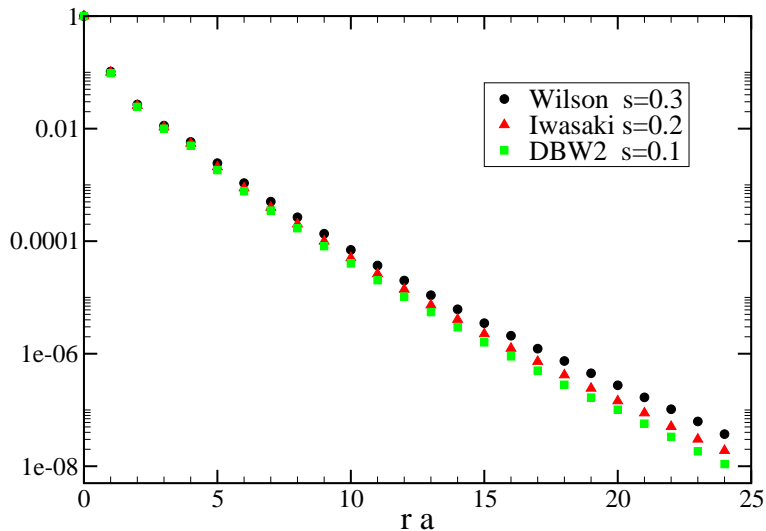


Figure 11: The localization of the overlap in gauge backgrounds generated with various gauge actions. The parameter s was chosen to make the operator as local as possible in the given gauge background.

needed in the case of DW fermions. As our results with the overlap suggest, improving the Domain Wall technology might be a better solution than going to extremes in tuning the gauge action.

B. Localization

We saw that the density of low modes of $A^\dagger A$ depends on the gauge action. There have been speculations on the connection between low modes of $A^\dagger A$ and the locality of the overlap [34, 35]. It is therefore interesting to compare the locality of the overlap in the different gauge backgrounds studied in the present work. This is done in Fig. 11, where the quantity

$$f(r) = \max \left\{ \|D_{ov}\psi(x)\| : \sum_{\mu} |x_{\mu}| = r \right\} \quad (27)$$

is plotted as a function of the so called “taxi driver distance”, $r = \sum_{\mu} |x_{\mu}|$ from a localized source $\psi_k(x) = \delta(x)\delta_{kj}$. This quantity was introduced in [34] to measure the (non)-locality of the overlap operator.

There are no surprises here. As seen in the figure, the general trend is that a large reduction in the number of small modes of $A^{\dagger}A$ results in a slight improvement of the locality of the overlap, in accordance with the results of [35], where different types and degrees of smearing were shown to have a similar effect.

VIII. CONCLUSIONS

In this paper we have investigated the reduction of lattice artifacts which can be achieved by altering the gauge field self-interaction and the fermion-gauge coupling. We focussed mostly – but not exclusively – on the reduction of lattice chiral symmetry breaking artifacts. Chiral improvement can be achieved by either altering the gauge action, or the fermion-gauge field coupling, or by a combination. That the two alterations produce similar effects is most starkly revealed by perturbation theory, where one sees that either effect alters the effective gluon propagator in fermionic Feynman diagrams. A variety of perturbative and nonperturbative tests reveal that a large c_1 in the gauge action can improve flavor symmetry violation for staggered fermions or the efficiency of implementing domain wall fermions or the overlap. However, a much more dramatic improvement can be achieved by replacing the thin link variable in the fermion action with smeared links. And the use of a large c_1 in the gauge action introduces a number of bad features into simulations: most notably a distortion of the heavy quark potential at short distance and long simulation time autocorrelations of the topological charge.

Acknowledgments

The work of T. D. and A. H. was supported by the U. S. Department of Energy with grant DE-FG03-95ER40894. The work of T. K. was supported by the EU’s Human Potential Program under contract HPRN-CT-2000-00145, by Hungarian science grant OTKA-T032501, and also partly by a Bolyai Fellowship.

-
- [1] D. Toussaint, Nucl. Phys. Proc. Suppl. **106**, 111 (2002), hep-lat/0110010.
 - [2] A. Hasenfratz and F. Knechtli, Comput. Phys. Commun. **148**, 81 (2002), hep-lat/0203010.
 - [3] G. P. Lepage, Phys. Rev. **D59**, 074502 (1999), hep-lat/9809157.
 - [4] K. Orginos and D. Toussaint (MILC), Phys. Rev. **D59**, 014501 (1999), hep-lat/9805009.
 - [5] K. Orginos, D. Toussaint, and R. L. Sugar (MILC), Phys. Rev. **D60**, 054503 (1999), hep-lat/9903032.
 - [6] A. Hasenfratz and F. Knechtli, Phys. Rev. **D64**, 034504 (2001), hep-lat/0103029.
 - [7] Y. Iwasaki (1983), uTHEP-118.
 - [8] A. Ali Khan et al. (CP-PACS), Nucl. Phys. Proc. Suppl. **83**, 360 (2000), hep-lat/9909075.
 - [9] A. Ali Khan et al. (CP-PACS), Phys. Rev. **D63**, 114504 (2001), hep-lat/0007014.
 - [10] T. Takaishi, Phys. Rev. **D54**, 1050 (1996).
 - [11] P. de Forcrand et al. (QCD-TARO), Nucl. Phys. **B577**, 263 (2000), hep-lat/9911033.
 - [12] K. Orginos (RBC), Nucl. Phys. Proc. Suppl. **106**, 721 (2002), hep-lat/0110074.
 - [13] A. Hasenfratz and A. Alexandru, Phys. Rev. **D65**, 114506 (2002), hep-lat/0203026.
 - [14] A. Alexandru and A. Hasenfratz (2002), hep-lat/0207014.
 - [15] P. Weisz, Nucl. Phys. **B212**, 1 (1983).
 - [16] M. Luscher and P. Weisz, Commun. Math. Phys. **97**, 59 (1985).
 - [17] D. W. Bliss, K. Hornbostel, and G. P. Lepage (1996), hep-lat/9605041.
 - [18] C. W. Bernard and T. DeGrand, Nucl. Phys. Proc. Suppl. **83**, 845 (2000), hep-lat/9909083.

- [19] C. Bernard et al. (MILC) (2002), hep-lat/0206016.
- [20] M. Albanese et al. (APE), Phys. Lett. **B192**, 163 (1987).
- [21] G. P. Lepage and P. B. Mackenzie, Phys. Rev. **D48**, 2250 (1993), hep-lat/9209022.
- [22] W.-j. Lee and S. R. Sharpe (2002), hep-lat/0208036.
- [23] T. DeGrand (2002), hep-lat/0210028.
- [24] T. DeGrand (MILC), Phys. Rev. **D60**, 094501 (1999), hep-lat/9903006.
- [25] R. Gupta, T. Bhattacharya, and S. R. Sharpe, Phys. Rev. **D55**, 4036 (1997), hep-lat/9611023.
- [26] R. G. Edwards, U. M. Heller, and T. R. Klassen, Nucl. Phys. **B517**, 377 (1998), hep-lat/9711003.
- [27] A. Hasenfratz, R. Hoffmann, and F. Knechtli (2001), hep-lat/0110168.
- [28] C. Gattringer, R. Hoffmann, and S. Schaefer (2001), hep-lat/0112024, accepted for publication in Phys. Rev. D.
- [29] S. Necco (2002), hep-lat/0208052.
- [30] T. DeGrand, A. Hasenfratz, and T. G. Kovacs, Nucl. Phys. **B505**, 417 (1997), hep-lat/9705009.
- [31] A. Hasenfratz and C. Nieter, Phys. Lett. **B439**, 366 (1998), hep-lat/9806026.
- [32] A. Hasenfratz, Phys. Rev. **D64**, 074503 (2001), hep-lat/0104015.
- [33] T. Schafer and E. V. Shuryak, Rev. Mod. Phys. **70**, 323 (1998), hep-ph/9610451.
- [34] P. Hernandez, K. Jansen, and M. Luscher, Nucl. Phys. **B552**, 363 (1999), hep-lat/9808010.
- [35] T. G. Kovacs (2002), hep-lat/0209125.